

Spin Transport in Nanowires Synthesized Using Anodic Nanoporous Alumina Films

Supriyo Bandyopadhyay

Abstract

Spin transport in restricted dimensionality structures (e.g., nanowires) have unusual features not observed in bulk samples. One popular method to synthesize nanowires of different materials is to electrodeposit them selectively within nanometer diameter pores in anodic alumina films. Different materials can be sequentially deposited within the pores to form nanowire “spin valves” consisting of a spacer nanowire sandwiched between two ferromagnetic nanowires. This construct allows one to study spin transport in the spacer nanowire, with the ferromagnetic contacts acting as spin injector and detector. Some of our past work related to the study of spin transport in organic and inorganic nanowire spin valves produced using nanoporous anodic alumina films is reviewed in this chapter.

Keywords: spin transport, nanowires, nanoporous anodic alumina films, self-assembly

1. Introduction

The use of anodic porous alumina films as templates to fabricate nanowires of different materials has a long history [1–15]. Such films have been used to fabricate organic [3], semiconducting [4] and metallic [6] nanowires in our group over the past three decades. While these structures have been used to demonstrate a wide variety of optical [7–9], magnetic [10, 11] and electronic [12–15] phenomena and devices, here we focus on spin transport properties investigated in nanowire “spin valves” fabricated by sequentially electrodepositing a ferromagnetic material, a semiconductor/metal/organic, and finally another ferromagnet selectively within the nanopores of anodic alumina films.

Figure 1 shows the schematic of a vertically standing array of nanowire spin-valves fabricated by electrodepositing different materials sequentially within the nanopores of an anodic alumina film.

To produce the nanoporous anodic film, first, a commercial grade aluminum foil of thickness 0.1 mm is diced into 2×2 cm coupons. Each coupon is electropolished in a solution of perchloric acid, ethanol, butyl cellusolve and distilled water to reduce the surface roughness to about 3 nm [16] which gives the surface a shiny appearance as shown in **Figure 2**. The electropolishing is carried out at 40 V dc in six intervals of 5 s each in order to not overheat the electropolishing solution. Next, the electropolished foil is rinsed in distilled water and anodized in an anodizing bath (**Figure 3a**) in 0.3 M oxalic acid using the foil as the anode and a platinum grid

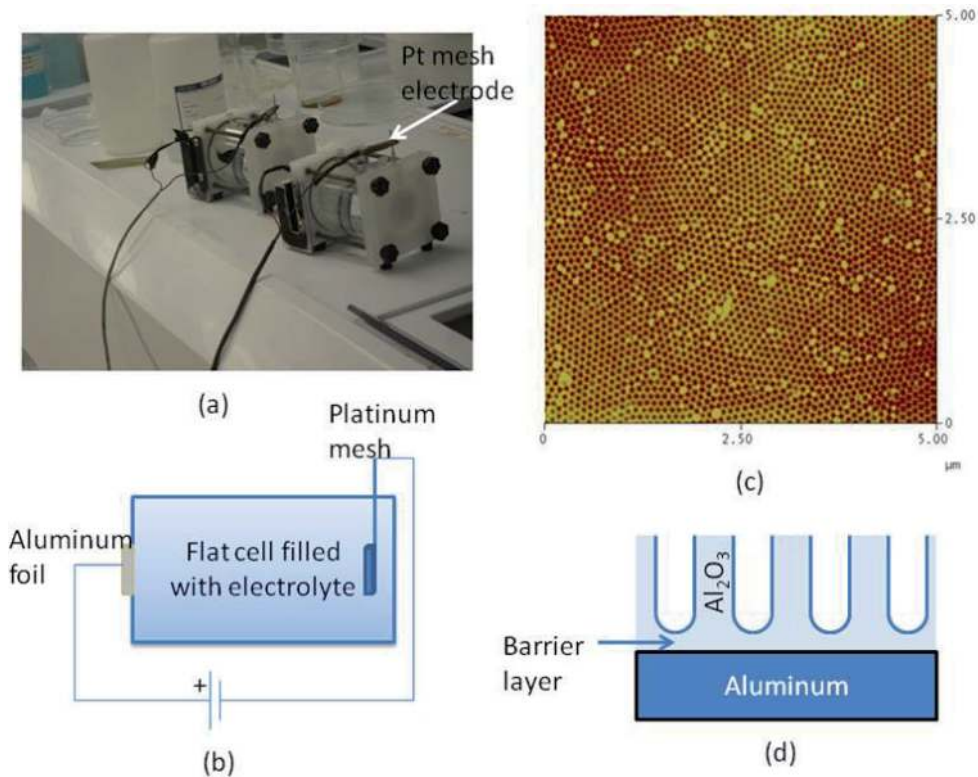


Figure 3. (a) The anodizing flat cells, (b) the anodizing configuration where the aluminum foil is used as the anode and a platinum mesh as the cathode, (c) an atomic force micrograph of the nanoporous film formed after anodization. There is excellent ordering of the pores within domains of size $\sim 1 \mu\text{m}$ and (d) cross-section of the pores showing the barrier layers which are later removed by soaking in phosphoric acid.

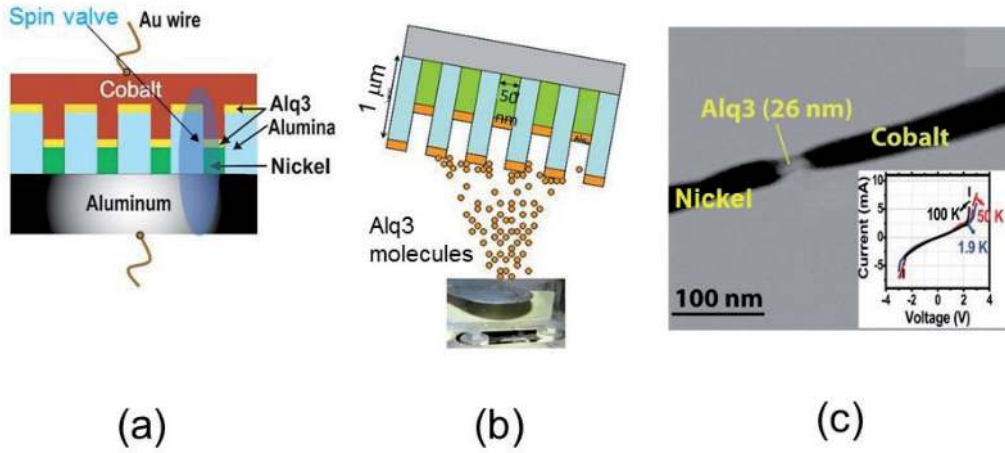
current to flow. The accumulated metal ions are deionized ($\text{Co}^{2+} + 2e^- = \text{Co}$) and are deposited within the pores. The spacer layer can also be electrodeposited by using appropriate solutions. For example, the procedure for depositing CdS is described in Refs. [13, 14]. Organics can be evaporated [3] or electrosprayed selectively within the pores [9]. In the end, we obtain a tri-layered nanowire of ferromagnet-spacer-ferromagnet as shown in **Figure 1**, constituting a nanowire spin valve. For electrical contacting, a metallic layer is deposited on top of the structure using electron beam evaporation. This layer and the bottom aluminum substrate are used as contacts and wires can be attached to these layers using silver paste.

2. Spin transport in nanowire spin valves formed in nanoporous alumina templates

2.1 Spin transport in organic nanowire spin valves

Organic nanowire spin valves were made of cobalt, Alq₃ (tris-(8-hydroxyquinolinolato) aluminum) and nickel by first electrodepositing 500 nm of Ni within 50-nm diameter pores, then evaporating Alq₃ through a 1 mm² window in a mask at a base pressure of 10^{-7} Torr, and then evaporating Co on top without breaking vacuum. Alq₃ seeps into the pores by capillary action upon evaporation. The fact that it is a short stranded molecule with low molecular weight helps in transporting the molecules inside the pores.

Figure 4 shows a schematic of the structure formed, along with a transmission electron micrograph (TEM) of a single nanowire spin valve that is produced within


Figure 4.

(a) Schematic of the organic nanowire spin valves, (b) evaporation of Alq₃ is carried out by tilting the sample by 15° with respect to the source to get the best results, (c) transmission electron micrograph of a single nanowire spin valve. The inset shows the measured current-voltage characteristic of an array of spin valves at two different temperatures. The non-linear characteristic shows that the contacts between the ferromagnets and organic have a Schottky character, indicating that Schottky barriers form at these interfaces. Tunneling through the Schottky barriers aids spin injection and detection at the ferromagnetic contacts. Figures (a) and (c) are reproduced from Ref. [16].

a pore. The micrograph was obtained by releasing the spin valves from the alumina matrix by dissolving out the latter in hot chromic/phosphoric acid and recapturing the released wires on a TEM grid for imaging.

Longitudinal magnetoresistance traces of an ensemble of organic nanowire spin valves, measured at three different temperatures are shown in **Figure 5(a)**. From the heights of the peaks shown in the traces, the spin diffusion length can be estimated using the modified Julliere relation [17].

$$\frac{\Delta R}{R} = \frac{2P_1P_2e^{-d/L_s}}{1 - P_1P_2e^{-d/L_s}} \quad (1)$$

where ΔR is the height of the magnetoresistance peak measured from the baseline, R is the baseline resistance, P_1 and P_2 are the spin polarizations in the Co and Ni contacts, d is the length of the spacer layer (26 nm from **Figure 4**), and L_s is the spin diffusion length in Alq₃. This last quantity is plotted as a function of temperature in the top panel of **Figure 5(b)**.

From the spin diffusion length, we can estimate the spin relaxation time using the relation

$$\tau_s = \frac{q^2 L_s^2}{kT\mu}, \quad (2)$$

where q is the electronic charge, kT is the thermal energy and μ is the mobility of carriers in Alq₃. Since the mobility in the organic is determined by carrier hopping, it is likely to be relatively independent of temperature. From the reported values of the mobility in Alq₃, we have found the extremum values of the spin relaxation time in the organic and these are plotted as a function of temperature in **Figure 5(b)**. These times are exceptionally long, perhaps among the longest reported in any solid above liquid nitrogen temperature (77 K). The reason why these times are so long is because Alq₃ is composed primarily of hydrocarbons which have low atomic number Z and hence weak spin-orbit interaction (the interaction strength is proportional to Z^4). The weak interaction preserves spin coherence over long durations, making organics a preferred platform for spintronics in some applications.

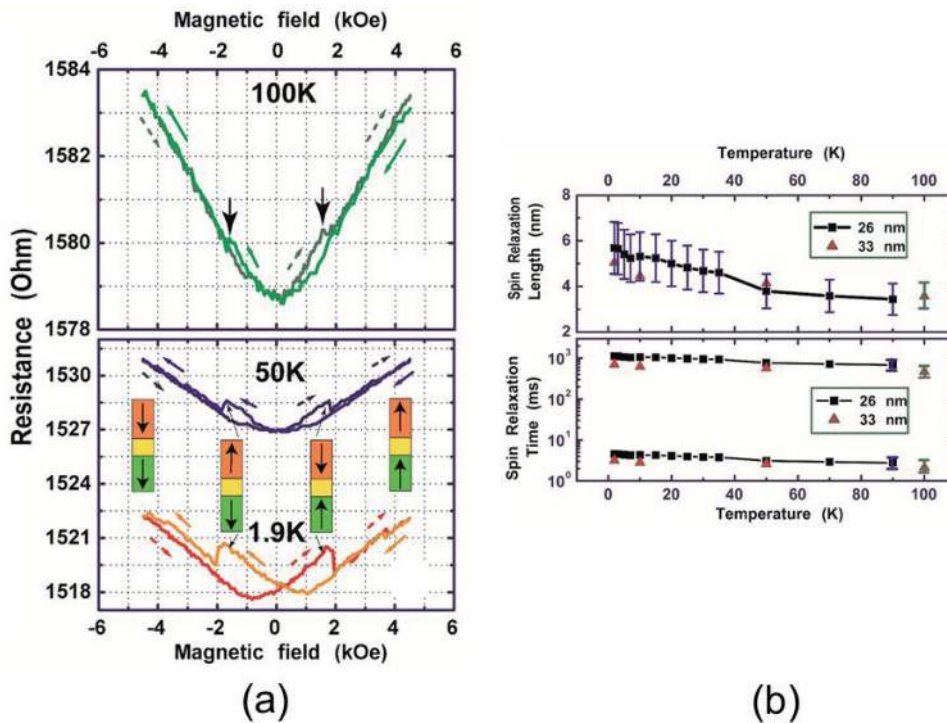


Figure 5. (a) Longitudinal magnetoresistance traces of an ensemble of spin valves measured at three different temperatures, (b) the estimated spin relaxation lengths and times as a function of temperature for two different sets of samples with spacer layer thicknesses of 26 and 33 nm. In the lower panel, the extremum values are shown for the spin relaxation times. Reproduced from Ref. [16].

There is a bit of controversy regarding the primary mechanism responsible for spin relaxation in an organic like Alq_3 . While Ref. [16] proposed that the main mechanism is the Elliott-Yafet spin relaxation [18], there is a strong differing opinion that it is hyperfine nuclear interaction [19]. The electric field dependence of the spin relaxation time (or spin diffusion length) observed in Ref. [3] speaks against hyperfine interaction and is more consistent with Elliott-Yafet relaxation. Recently, this view was concurred with in the context of spin transport in organic single crystal semiconductors [20].

2.2 Spin transport in semiconductor nanowire spin valves

Nanowire spin valves (diameter = 50 nm) with germanium as the spacer and Co, Ni as the ferromagnetic contacts have also been produced in our group using sequential electrodeposition of the constituent elements in 50 nm diameter pores in anodic alumina films. The Co and Ni were electrodeposited from aqueous solutions of NiSO_4 and CuSO_4 . Ge was electrodeposited using the ionic liquid 1-butyl-3-methylimidazolium hexafluorophosphate (BMIM-PF_6), GeI_4 salts and dimethyl sulfoxide (DMSO) [21]. A gold top contact was deposited by electron beam evaporation and the Al foil was contacted from the back to electrically access an ensemble of spin valves as shown in **Figure 6(a)**. For characterization, the nanowire spin valves were released from their alumina hosts by dissolving out the alumina in hot chromic/phosphoric acid and then capturing the released spin valves in TEM grid for imaging. **Figure 6(b)** shows a transmission electron micrograph of a single spin valve that forms within a single pore.

Longitudinal magnetoresistance traces of these spin valve samples were obtained and from the spin valve peaks, the spin relaxation length (L_s) and time (τ_s)

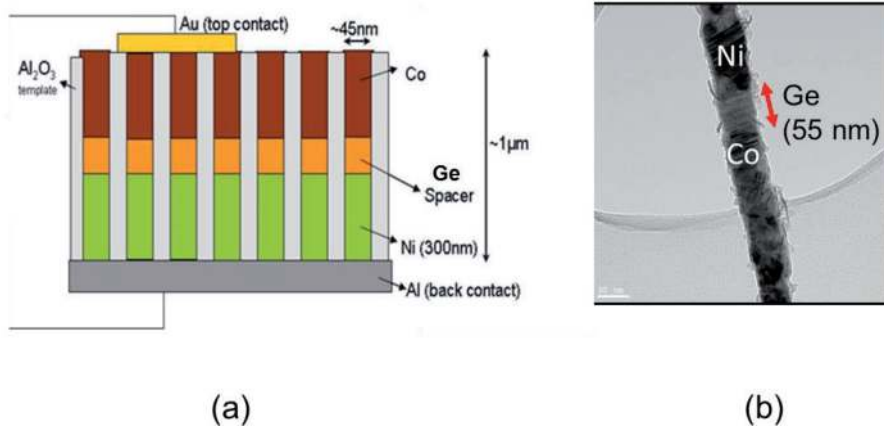


Figure 6. (a) An array of vertically standing nanowire spin valves with Ge spacer hosted in an alumina matrix and (b) transmission electron micrograph of a single nanowire spin valve. Credit: Sridhar Patibandla.

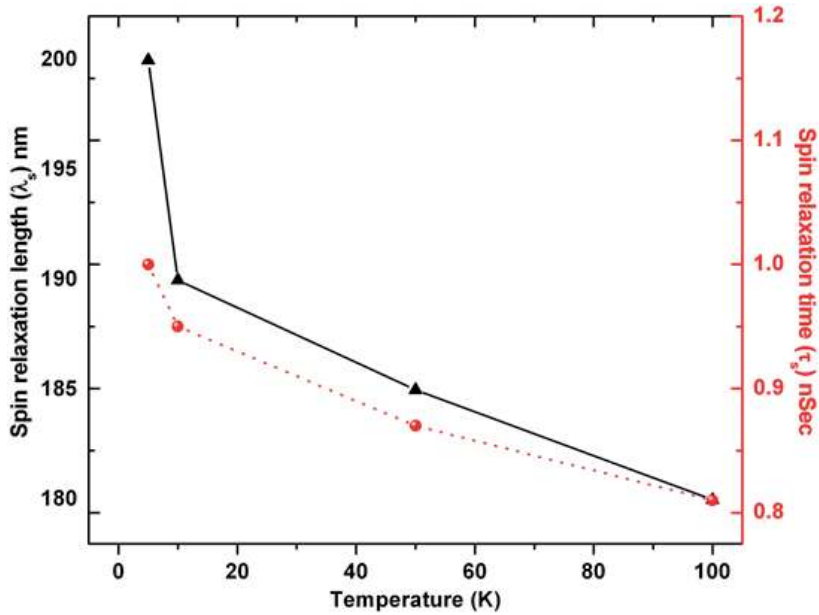


Figure 7. Spin relaxation length and time in Ge nanowires as a function of temperature. Credit: Sridhar Patibandla.

were obtained following Eqs. (1) and (2). These quantities are plotted in **Figure 7** as a function of temperature.

Interestingly, the spin relaxation length at 4.2 K is ~200 nm which is longer than that reported in carbon nanotubes (130 nm) at that temperature [22]. Even at liquid nitrogen temperature (77 K), the spin relaxation length is over 180 nm, which makes Ge nanowires viable for spin-transistor type applications.

Germanium is an indirect gap semiconductor with the lowest conduction band valley at the L-point where the electron wavefunctions have some *p*-type character leading to non-zero intrinsic spin-orbit coupling. This should be the dominant spin relaxation mechanism in the Ge spacer layer since the Dresselhaus interaction [23] should be weak or non-existent owing to the fact that the Ge crystal is centrosymmetric. The Rashba interaction [24] should also be weak because of the absence of strong symmetry breaking by electric fields. The most common isotope of germanium ^{74}Ge has no net nuclear spin and hence hyperfine interaction with nuclear spins

should also be weak in a Germanium nanowire. This leaves the intrinsic spin-orbit interaction as the likely dominant source of spin relaxation. The spin orbit interaction can cause both Elliott-Yafet [18] and D'yakonov-Perel' [25] spin relaxation in germanium nanowires, although in our samples, the poor mobility caused by interface scattering makes the Elliot-Yafet mechanism more likely to be dominant.

2.3 Spin transport in InSb nanowire spin valves at room temperature

Most spin transport experiments in nanowire spin valves have been conducted at low temperatures where the spin diffusion length is long enough to exhibit observable spin transport effects. Spin transport at room temperature is rarely, if ever, studied because the short spin relaxation lengths at room temperature obscure most spin effects. However, practical devices based on spin transport would require room temperature operation. This begs the question as to when spin transport effects may be observable at room temperature. To answer this question, one needs to understand what are the dominant sources of spin relaxation in semiconductor nanowires (in a given circumstance) and what could be done to suppress them in order to slow down the spin relaxation rate at room temperature.

In most semiconductors, the dominant spin relaxation mechanism at room temperature is the D'yakonov-Perel' mechanism [25]. This mechanism accrues from spin-orbit interaction that acts as an effective (velocity-dependent) magnetic field for electrons [26]. The electron spins precess about this effective magnetic field while transiting through a semiconductor. Collisions change the magnitude and direction of an electron's velocity and hence the direction and magnitude of the effective magnetic field. The spins therefore precess about randomly changing axes (direction of the effective magnetic field) with random angular frequencies since the frequency of precession is proportional to the magnetic field strength. This randomness causes ensemble spin relaxation.

In a strictly *one-dimensional* semiconductor structure (quantum wire), where only a *single* transverse subband is occupied by electrons, the D'yakonov-Perel' mechanism is completely suppressed as long as the axis of the nanowire is along certain principal crystallographic directions [26]. This would increase the spin relaxation time (and length) considerably, and may make spin effects observable at room temperature. In order to verify this prediction, we prepared InSb nanowire spin valves of 50 nm diameter in nanoporous alumina films. Since InSb has a very small electron effective mass, the energy spacing between subbands in a 50 nm diameter InSb nanowire is large enough that only a single subband could be occupied at room temperature. This would suppress the D'yakov-Perel' mechanism in an InSb nanowire and might make spin effects observable at room temperature.

Vertically standing arrays of nanowire spin valves consisting of Co-InSb-Ni and encased in an alumina matrix were produced by sequentially electrodepositing these materials within 50-nm diameter nanopores using dc electrodeposition. The finished structure looks like that in **Figure 6(a)**, except the spacer layer is InSb instead of Ge. InSb is electrodeposited from a solution of 0.15 M InSO_4 , 0.1 M SbCl_3 , 0.17 M $\text{Na}_3\text{C}_6\text{H}_5\text{O}_7$ and 0.36 M $\text{C}_6\text{H}_8\text{O}_7$ (citric acid). The Co and InSb depositions were carried out at 3 V dc for 1 min each whereas the Ni electrodeposition was carried out at 5 V dc for 6 min to slightly overfill the pores and make the Ni spill out on the surface. These structures were contacted from the top and bottom with copper wires attached with silver paste.

We measured both the longitudinal and transverse magnetoresistance of the spin valve samples at room temperature using an electromagnet. The longitudinal magnetoresistance was measured with the magnetic field pointing in the direction of the nanowire axis (which is also the direction of current flow during

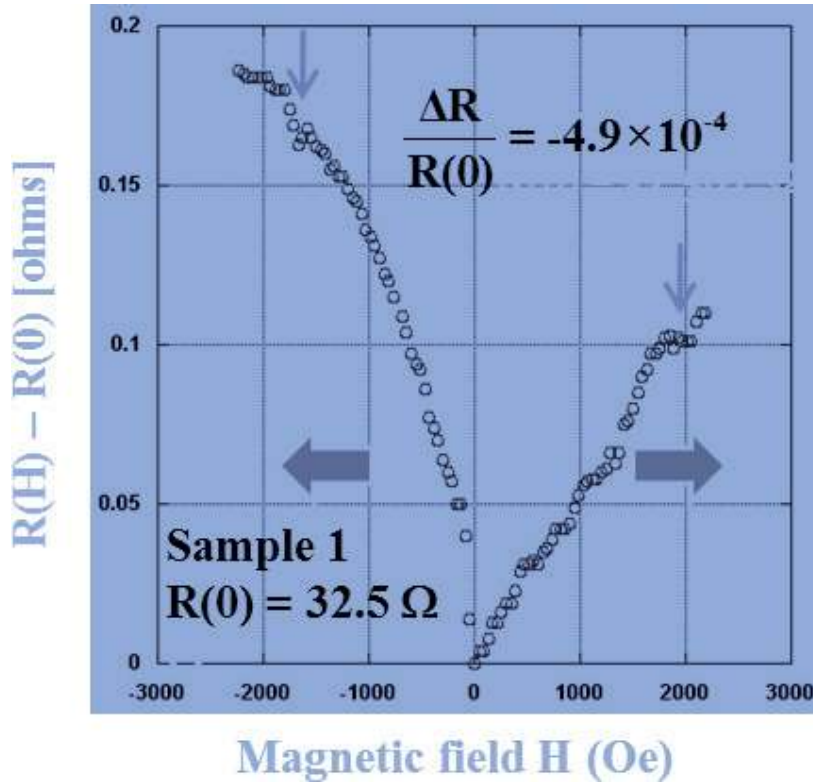


Figure 8. Longitudinal magnetoresistance of InSb nanowire spin valves at room temperature. The spin valve troughs are indicated with vertical arrows. Reproduced from Ref. [28] with permission of Wiley.

magnetoresistance measurement). The transverse magnetoresistance was measured with the magnetic field perpendicular to the direction of current flow (and hence perpendicular to the nanowire axes).

Figure 8 shows the longitudinal magnetoresistance traces with the positive and negative field segments corresponding to forward and reverse scans of the magnetic field. There are two shallow “troughs” marked with vertical arrows. These are the tell-tale spin valve troughs. They are the counterparts of the spin valve peaks seen in **Figure 5**. Normally the spin valve effect would result in the magnetoresistance exhibiting peaks between the coercive fields of the two ferromagnetic contacts, but if there are defects close to either contact that electrons can resonantly tunnel through, then the spin polarization of that contact can be reversed, resulting in a trough as opposed to a peak in the longitudinal magnetoresistance [27]. From the measured depths of these troughs (ΔR), we can obtain the spin relaxation length L_s using Eq. (1) if we know what the spacer layer length L is. Transmission electron microscopy revealed the spacer layer length in the samples to be ~ 20 nm. The ratio L_s/L in the sample shown in **Figure 8** was found to be 0.29, indicating that the spin relaxation length in the InSb nanowire is 5.88 nm at room temperature under equilibrium.

We calculated that the energy spacing between the two lowest subbands in the InSb nanowires is 3.9 kT at room temperature (101 meV) which would force 96% of the electrons to reside in the lowest subband at room temperature [28]. This means that the samples are almost strictly one dimensional quantum wires where the D'yakonov-Perel relaxation will be strongly suppressed [28]. The experimental observations in Ref. [28] confirmed this view.

Because of the strict one-dimensionality of our nanowires, we can relate the spin relaxation length L_s and the spacer layer length L to the spin relaxation time (τ_s) and the transit time through the spacer (τ_t) according to

$$\begin{aligned} L &= v_d \tau_t \\ L_s &= v_d \tau_s \end{aligned} \quad (3)$$

where v_d is the drift velocity of electrons in the spacer.

In order to determine the transit time through the spacer layer, we measured the transverse magnetoresistance and observed Hanle oscillations in the magnetoresistance traces [28].

To understand the origin of Hanle oscillations in the magnetoresistance, one can refer to **Figure 9**. The magnetic field is directed perpendicular to the axis of the nanowire spin valve. The ferromagnetic contacts are initially magnetized along the axis with a longitudinal magnetic field. Depending on the nature of the ferromagnets, this will align the magnetizations of the two contacts either parallel, or antiparallel, to each other, as shown in **Figure 9**. The left contact, connected to the negative pole of the battery, injects electrons into the nanowire spacer with their spins pointing to the right. The transverse magnetic field makes the spins precess in the plane normal to the magnetic field. If the spins precess through an angle that is an odd multiple of π , then the spins arriving at the right ferromagnetic contact will be either antiparallel (in the case of parallel contacts) or parallel (in the case of antiparallel contacts) to the magnetization of the right contact. In the former case, the spins will be blocked by the right contact and the resistance of the spin valve will be high. In the latter case, the spins will transmit through the right contact and the resistance will be low. The reader can easily understand that the situation will be opposite when the spins precess through an angle that is an even multiple of π .

If we continuously increase the magnetic field, that will increase the precessional frequency (and hence the angle Φ through which the spins precess as they traverse the spacer layer) linearly with the field. Every time Φ reaches an odd integral value of π , the resistance either peaks or ebbs depending on the situation just described. That will lead to oscillations in the transverse magnetoresistance. These are the Hanle oscillations.

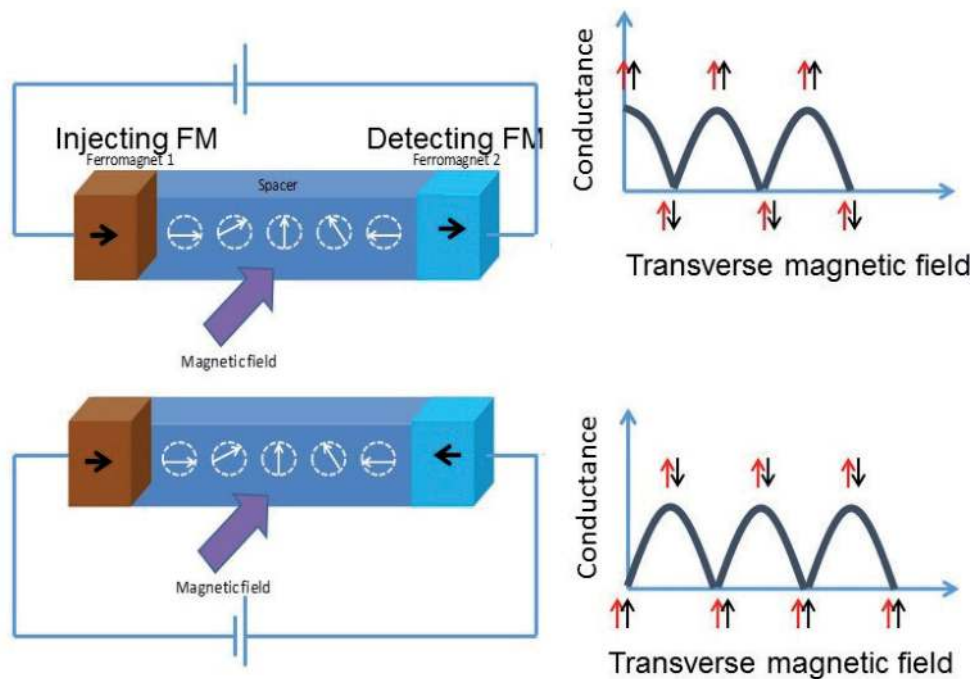


Figure 9. Origin of Hanle oscillations in the magneto conductance. The left panel explains the origin of the effect and the right panel shows the Hanle oscillations in the magneto conductance.

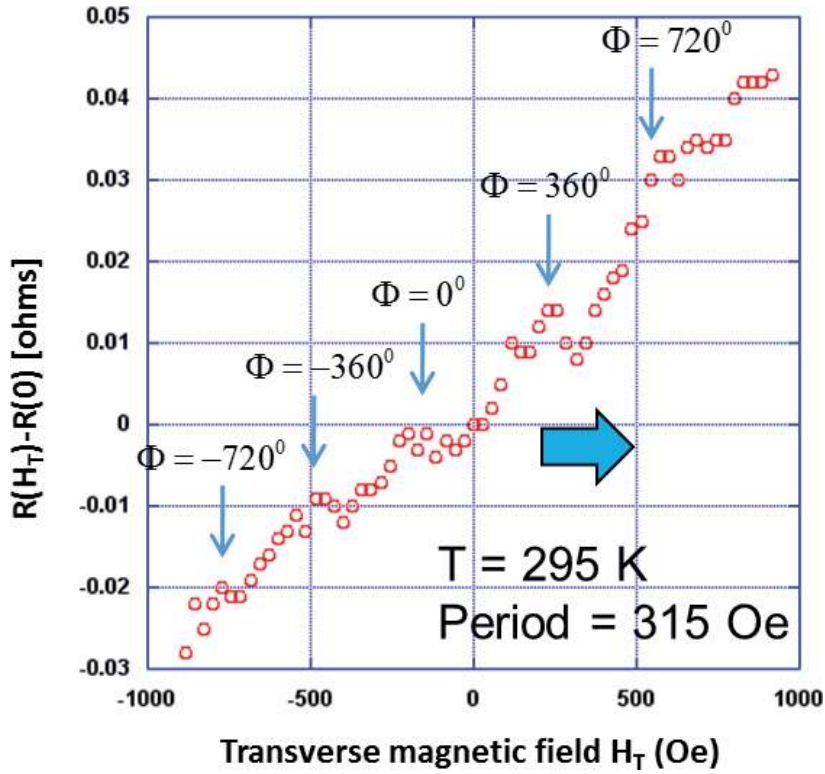


Figure 10. Hanle oscillations in the transverse magnetoresistance traces of the InSb nanowire samples at room temperature. Reproduced from Ref. [28] with permission of Wiley.

In **Figure 10**, we show the observed Hanle oscillations at room temperature. The measured period of the oscillations in the transverse magnetic field is 315 Oe.

The transit time through the spacer layer is related to the oscillation period according to

$$\tau_t = \frac{h}{|g|\mu_B B_0}, \quad (4)$$

where h is the Planck constant, g is the Landé g -factor of InSb, μ_B is the Bohr magneton and B_0 is the period of the oscillation.

From Eq. (4), using $B_0 = 315$ Oe, we find that the average transit time through the spacer layers of the spin valves is 44 ps. Using this value in Eq. (3), we deduce that the drift velocity of electrons in the spacer layer is 454 m/s. From Eq. (3), we can then determine that the spin relaxation time in the InSb spacer layer is 13 ps. This is approximately one order of magnitude larger than that reported in InSb or InAs quantum wells [29, 30].

3. Conclusions

In this chapter, I have described some spin transport experiments in nanowire spin valves produced by sequentially electrodepositing various materials (ferromagnet-spacer-ferromagnet) within nanopores of anodic alumina films. These experiments have revealed intriguing and important features of spin transport in restricted dimensionality systems. They have also demonstrated the immense capability afforded by electrochemical self-assembly methods.

Acknowledgements

The work described here has been supported by various grants through the US National Science Foundation at various times. Most of the work was carried out by my erstwhile Ph.D. students, post-doctoral mentees and high-school interns— Dr. Sridhar Patibandla (now at Intel Corporation, USA), Prof. Sandipan Pramanik (now at University of Alberta, Canada), Dr. Carmen-Gabriela Stefanita (now at IBM Data Science, USA), Dr. Iftexhar Hossain (now at Eastman Chemicals, USA), Dr. Hasnain Ahmad (now at IMEC, Belgium) and Mr. Saumil Bandyopadhyay (now at MIT, USA). I am also grateful to my collaborators Prof. Marc Cahay from University of Cincinnati, and Profs. Jayasimha Atulasimha and Gary C. Tepper from Virginia Commonwealth University.


The author declares no competing interest.

Author details

Supriyo Bandyopadhyay
Department of Electrical and Computer Engineering, Virginia Commonwealth University, Richmond, VA, USA

*Address all correspondence to: sbandy@vcu.edu

IntechOpen

© 2020 The Author(s). Licensee IntechOpen. Distributed under the terms of the Creative Commons Attribution - NonCommercial 4.0 License (<https://creativecommons.org/licenses/by-nc/4.0/>), which permits use, distribution and reproduction for non-commercial purposes, provided the original is properly cited. 

References

- [1] Masuda H, Nishio K. Synthesis and applications of highly ordered anodic porous alumina. In: Adachi M, Lockwood DJ, editors. *Self-Organized Nanoscale Materials, Nanostructure Science and Technology*. New York: Springer; 2006. pp. 296-312
- [2] Huber CA, Huber TE, Sadoqi M, Lubin JA, Manalis S, Prater CB. Nanowire array composites. *Science*. 1994;**263**:800-802
- [3] Pramanik S, Bandyopadhyay S, Garre K, Cahay M. Normal and inverse spin-valve effect in organic semiconductor nanowires and the background monotonic magnetoresistance. *Physical Review B*. 1998;**74**:235329
- [4] Ramanathan S, Patibandla S, Bandyopadhyay S, Edwards JD, Anderson J. Fluorescence and infrared spectroscopy of electrochemically self-assembled ZnO nanowires: Evidence of the quantum confined stark effect. *Journal of Materials Science: Materials in Electronics*. 2006;**17**:651-655
- [5] Iwasaki T, Motoi T, Den T. Multi-walled carbon nanotubes growth in anodic alumina nanoholes. *Applied Physics Letters*. 1999;**75**:2044-2046
- [6] Zeng H, Michalski S, Kirby RD, Sellmyer DJ, Menon L, Bandyopadhyay S. Effects of surface morphology on magnetic properties of Ni nanowire arrays in self-ordered porous alumina. *Journal of Physics: Condensed Matter*. 2002;**14**:715-721
- [7] Kouklin N, Menon L, Wong AZ, Thompson DW, Woollam JA, Williams PF, et al. Giant photoresistivity and optically controlled switching in self-assembled nanowires. *Applied Physics Letters*. 2001;**79**:4423-4425
- [8] Ramanathan S, Patibandla S, Bandyopadhyay S, Anderson J, Edwards JD. Fluorescence spectroscopy of electrochemical self-assembled ZnSe and Mn:ZnSe nanowires. *Nanotechnology*. 2008;**19**:195601
- [9] Sarkar S, Kanchibotla B, Nelson JD, Edwards JD, Anderson J, Tepper GC, et al. Giant increase in the metal-enhanced fluorescence of organic molecules in nanoporous alumina templates and large molecule-specific red/blue shift of the fluorescence peak. *Nano Letters*. 2014;**14**:5973-5978
- [10] Zeng H, Zheng M, Skomski R, Sellmyer DJ, Liu Y, Menon L, et al. Magnetic properties of self-assembled Co nanowires of varying length and diameter. *Journal of Applied Physics*. 2000;**87**:4718-4720
- [11] Zeng H, Skomski R, Menon L, Liu Y, Bandyopadhyay S, Sellmyer DJ. Structure and magnetic properties of ferromagnetic nanowires self-assembled arrays. *Physical Review B*. 2002;**65**:134426
- [12] Kouklin N, Bandyopadhyay S, Tereshin S, Varfolomeev A, Zarestky D. Electronic bistability in electrochemically self-assembled quantum dots: A potential non-volatile random access memory. *Applied Physics Letters*. 2000;**76**:460-462
- [13] Kouklin N, Menon L, Bandyopadhyay S. Room-temperature single electron charging in electrochemically synthesized semiconductor quantum dot and wire array. *Applied Physics Letters*. 2002;**80**:1649-1651
- [14] Varfolomeev A, Zarestky D, Pokalyakin V, Tereshin S, Pramanik S, Bandyopadhyay S. Admittance of CdS nanowires embedded in porous alumina template. *Applied Physics Letters*. 2006;**88**:113114

- [15] Cahay M, Garre K, Fraser JW, Lockwood DJ, Semet V, Binh VT, et al. Characterization and field emission properties of lanthanum monosulfide nanoprotrusion arrays obtained by pulsed laser deposition on self-assembled nanoporous alumina templates. *Journal of Vacuum Science and Technology B*. 2007;**25**:594-603
- [16] Pramanik S, Stefanita C-G, Patibandla S, Bandyopadhyay S, Garre K, Harth N, et al. Observation of extremely long spin relaxation times in an organic nanowire spin valve. *Nature Nanotechnology*. 2007;**2**:216-219
- [17] Julliere M. Tunneling between ferromagnetic films. *Physics Letters A*. 1975;**54**:225-226
- [18] Elliott RJ. Theory of the effect of spin-orbit coupling on magnetic resonance in some semiconductors. *Physics Review*. 1954;**96**:266-279
- [19] Bobbert PA, Wagemans W, van Oost FWA, Koopmans B, Wohlgenannt M. Theory for spin diffusion in disordered organic semiconductors. *Physical Review Letters*. 2009;**102**:156604
- [20] Tsurumi J, Matsui H, Kubo T, Häusermann R, Mitsui C, Okamoto T, et al. Coexistence of ultra-long spin relaxation time and coherent charge transport in organic single crystal semiconductors. *Nature Physics*. 2017;**13**:994-998
- [21] Patibandla S, Pramanik S, Bandyopadhyay S, Tepper GC. Spin relaxation in a germanium nanowire. *Journal of Applied Physics*. 2006;**100**:044303
- [22] Tsukogoshi K, Alphenaar BW, Ago H. Coherent transport of electron spin in a ferromagnetically contacted carbon nanotube. *Nature*. 1999;**401**:572
- [23] Dresselhaus G. Spin-orbit coupling effects in zinc blende structures. *Physics Review*. 1955;**100**:580
- [24] Bychkov YA, Rashba EI. Oscillatory effects and the magnetic susceptibility of carriers in inversion layers. *Journal of Physics C: Solid State Physics*. 1984;**17**:6039-6045
- [25] D'yakonov MI, Perel' VI. Spin orientation of electrons associated with the interband absorption of light in semiconductors. *Soviet Physics—JETP*. 1971;**33**:1053
- [26] Bandyopadhyay S, Cahay M. *Introduction to Spintronics*. 2nd ed. Boca Raton: CRC Press; 2015
- [27] Tsymbal EY, Sokolov A, Sabirianov IF, Doudin B. Resonant inversion of tunneling magnetoresistance. *Physical Review Letters*. 2003;**90**:186602
- [28] Bandyopadhyay S, Hossain MI, Ahmad H, Atulasimha J, Bandyopadhyay S. Coherent spin transport and suppression of spin relaxation in InSb nanowires with single subband occupancy at room temperature. *Small*. 2014;**10**:4379-4385
- [29] Bhowmick M, Kini RN, Nontapot K, Goel N, Chung SJ, Mishima TD, et al. Probe of interband relaxations of photo-excited carriers and spins in InSb based quantum wells. *Physics Procedia*. 2010;**3**:1161-1165
- [30] Olesberg JT, Lau WH, Flatté ME, Yu C, Altunkaya E, Shaw EM, et al. Interface contributions to spin relaxation in a short period InAs/GaSb superlattice. *Physical Review B*. 2001;**64**:201301(R)